






## RESEARCH ARTICLE

WILEY

# *Helichrysum stoechas* (L.) Moench reduces body weight gain and modulates mood disorders via inhibition of silent information regulator 1 (SIRT1) by arzanol

Vittoria Borgonetti<sup>1,2</sup>  | Clarissa Caroli<sup>3,4</sup> | Paolo Governa<sup>5,6</sup>  |  
Brighenti Virginia<sup>3</sup> | Federica Pollastro<sup>7</sup> | Silvia Franchini<sup>3</sup> | Fabrizio Manetti<sup>5</sup>  |  
Francisco Les<sup>8,9</sup> | Victor López<sup>8,9</sup> | Federica Pellati<sup>3</sup>  | Nicoletta Galeotti<sup>1</sup> 

<sup>1</sup>Department of Neuroscience, Psychology, Drug Research and Child Health (NEUROFARBA), Section of Pharmacology and Toxicology, University of Florence, Florence, Italy

<sup>2</sup>Department of Molecular Medicine and Neuroscience, Scripps Research Institute, La Jolla, California, USA

<sup>3</sup>Department of Life Sciences, University of Modena and Reggio Emilia, Modena, Italy

<sup>4</sup>Clinical and Experimental Medicine PhD Program, University of Modena and Reggio Emilia, Modena, Italy

<sup>5</sup>Department of Biotechnology, Chemistry and Pharmacy, University of Siena, Siena, Italy

<sup>6</sup>Department of Integrative Structural and Computational Biology, Scripps Research Institute, La Jolla, California, USA

<sup>7</sup>Department of Pharmaceutical Sciences, University of Eastern Piedmont, Novara, Italy

<sup>8</sup>Department of Pharmacy, Faculty of Health Sciences, Universidad San Jorge, Zaragoza, Spain

<sup>9</sup>Instituto Agroalimentario de Aragón, IA2, Universidad de Zaragoza-CITA, Zaragoza, Spain

## Correspondence

Federica Pellati, Department of Life Sciences, University of Modena and Reggio Emilia, Via Giuseppe Campi 103, 41125 Modena, Italy.  
Email: [federica.pellati@unimore.it](mailto:federica.pellati@unimore.it)

Nicoletta Galeotti, Department of Neuroscience, Psychology, Drug Research and Child Health (NEUROFARBA), Section of Pharmacology and Toxicology, University of Florence, Viale G. Pieraccini 6, 50139 Florence, Italy.  
Email: [nicoletta.galeotti@unifi.it](mailto:nicoletta.galeotti@unifi.it)

## Abstract

The prevalence of obesity is steadily rising, making safe and more efficient anti-obesity treatments an urgent medical need. Growing evidence correlates obesity and comorbidities, including anxiety and depression, with the development of a low-grade inflammation in peripheral and central tissues. We hypothesized that attenuating neuroinflammation might reduce weight gain and improve mood. We investigated the efficacy of a methanolic extract from *Helichrysum stoechas* (L.) Moench (HSE), well-known for its anti-inflammatory properties, and its main constituent arzanol (AZL). HPLC-ESI-MS<sup>2</sup> and HPLC-UV were used to characterize the extract. HSE effects on mood and feeding behavior was assessed in mice. The mechanism of action of HSE and AZL was investigated in hippocampus samples and SH-SY5Y cells by western blotting and immunofluorescence. Oral administration of HSE for 3 weeks limited weight gain with no significant decrease in food intake. HSE produced an anxiolytic-like and antidepressant-like phenotype comparable to diazepam and amitriptyline, respectively, in the absence of

**Abbreviations:** ACN, acetonitrile; AMI, amitriptyline; ANOVA, analysis of variance; ARRIVE, animal research: reporting of in vivo experiments; AZL, arzanol; CCK-8, coeliacostokine-8; CMC, carboxymethylcellulose; CNS, central nervous system; DIAZ, diazepam; DMSO, dimethyl sulfoxide; EDTA, ethylenediaminetetraacetic acid; EGTA, ethylene glycol tetraacetic acid; FoxO1, Forkhead Box O1 transcription factor; HPLC, high performance liquid chromatography; HRP, horseradish peroxidase; HSE, *Helichrysum stoechas* (L.) Moench extract; IC<sub>50</sub>, half-maximal inhibitory concentration; LDB, light dark box; MeOH, methanol; NORT, Novel Object Recognition Test; OF, open field; PBS, phosphate buffered saline; PBST, phosphate-buffered saline with 1% tween 20; PCC, Pearson's coefficient; PMSF, phenylmethylsulfonyl fluoride; PNFF, *p*-nitrophenylphosphate; RIPA, radioimmunoprecipitation assay buffer; SD, standard deviation; SEM, standard error of the mean; SIRT1, silent information regulator 1; SRB, Sulforhodamine B assay; SST, sucrose splash test; TST, tail suspension test; VEH, vehicle.

This is an open access article under the terms of the [Creative Commons Attribution-NonCommercial](https://creativecommons.org/licenses/by-nc/4.0/) License, which permits use, distribution and reproduction in any medium, provided the original work is properly cited and is not used for commercial purposes.

© 2023 The Authors. *Phytotherapy Research* published by John Wiley & Sons Ltd.

locomotor and cognitive impairments and induced neuroprotective effects in glutamate-exposed SH-SY5Y cells. A dose-dependent reduction of SIRT1 expression was detected in SH-SY5Y cells and in hippocampal samples from HSE-treated mice. The inhibition of the SIRT1-FoxO1 pathway was induced in the hypothalamus. Molecular docking studies proposed a mechanism of SIRT1 inhibition by AZL, confirmed by the evaluation of inhibitory effects on SIRT1 enzymatic activity. HSE limited weight gain and comorbidities through an AZL-mediated SIRT1 inhibition. These activities indicate HSE an innovative therapeutic perspective for obesity and associated mood disorders.

#### KEYWORDS

anxiety, arzanol, depression, *Helichrysum stoechas*, obesity, SIRT1 inhibitor

## 1 | INTRODUCTION

Obesity is now reaching worldwide epidemic proportions (Blüher, 2019), representing a major health problem associated with a reduction of quality of life, disability, and shortened life span (Heymsfield & Wadden, 2017). The prevalence of this condition is rising steadily (Kelly et al., 2008) and it has nearly tripled since 1975. The World Health Organization (WHO) has estimated that approximately one-third of the adult population worldwide was overweight in 2016. Obesity is defined as having a body mass index (BMI) of 30 kg/m<sup>2</sup> or higher according to the WHO. However, the wide range of associated disorders makes it far from being simply defined as weight gain.

Growing evidence indicates obesity as a multifactorial condition that results in the development of low-grade inflammation in the adipose tissue (Michailidou et al., 2022). This inflammation gradually becomes systemic, contributing to the development of metabolic and vascular impairments, affecting the functionality of organs and tissues, including the central nervous system (CNS) (Lumeng & Saltiel, 2011). Interestingly, obese patients represent a population more prone to develop central disorders (Bruce-Keller et al., 2009). An increased incidence of CNS pathologies, such as dementia, stroke, and Alzheimer's disease, has emerged (Pugazhenthil et al., 2017), and overweight and obesity have been frequently associated with mood disorders, such as anxiety (Amiri & Behnezhad, 2019) and depression (Milaneschi et al., 2019). These neurological pathologies have different etiologies and pathophysiological manifestations, but they share a common biological mechanism, involving brain inflammation, i.e. neuroinflammation (Leng & Edison, 2021). Although the undoubted relevance of the psychological and behavioral factors in a bidirectional association between mood disorders and obesity, mounting evidence highlights the key role of biological factors involving an immune-inflammatory activation in the pathobiology of mood disorders (Troubat et al., 2021). Indeed, peripheral inflammation in obese subjects is translated into brain inflammation, leading to higher hippocampal and cortical expression of cytokines in obesity animal models (Erion et al., 2014), that alter neurotransmission systems involved in the pathophysiological processes of depression (Milaneschi et al., 2019). Thus, the attenuation of neuroinflammation might reduce obesity and exert antidepressant/anxiolytic effects, improving the overall condition of patients.

Despite the efficacy of the pharmacological agents for obesity, their clinical use is limited mainly because of the induction of undesirable side effects (Patel & Stanford, 2018), making safe and more efficient anti-obesity treatments urgently needed. The use of natural products to treat minor and major illnesses is increasing worldwide and the demand for natural anti-obesity drugs has been consistently raised in the last decade, mainly due to their favorable safety profile and lower cost. Some plant extracts exerting anti-inflammatory activity and a positive effect on lipid and glucose metabolism, such as green tea, aloe, turmeric, etc., have been reported to act as anti-obesity agents (Mopuri & Islam, 2017). In an effort of searching for innovative and effective interventions for obesity, we focused our research on identifying natural agents endowed with both anti-inflammatory and antidepressant/anxiolytic activity, that might reduce body weight and improve mood. Extracts from different species of *Helichrysum* have shown to possess an anti-inflammatory activity (Mao et al., 2017; Sala et al., 2010) and recent findings have reported the anxiolytic efficacy of a methanolic extract from *Helichrysum stoechas* (L.) Moench (HSE) after acute administration (Borgonetti, Les, et al., 2020).

We hypothesized that attenuating neuroinflammation might reduce weight gain and improve mood. Based on the well-known anti-inflammatory properties of *Helichrysum* species, the aim of the present study was to investigate the efficacy of HSE and its main constituent arzanol (AZL) on feeding behavior and mood alterations. HSE was fully characterized using chromatographic techniques and its capability to reduce body weight and to induce antidepressant- and anxiolytic-like activities was studied in animal models. The cellular and molecular mechanisms and the safety profile of HSE were also investigated.

## 2 | MATERIALS AND METHODS

### 2.1 | Plant material characterization

#### 2.1.1 | Plant material

*Helichrysum stoechas* (L.) Moench was collected in Villanueva de Gállego (Zaragoza, Spain) in June 2021 and the methanolic extract (HSE)

was obtained from the inflorescences by cold maceration with MeOH as previously reported (Les et al., 2017). The solvent was removed under vacuum at 37°C to obtain HSE. The plant material was authenticated by Dr. Víctor López and a voucher is kept at Universidad San Jorge herbarium with the reference number 002-2014.

## 2.1.2 | Chemicals and solvents

Acetonitrile (ACN), methanol (MeOH), and formic acid (HCOOH) were purchased from Sigma-Aldrich s.r.l. (Milan, Italy). Water (H<sub>2</sub>O) was purified by using a Milli-Q Plus185 system from Millipore (Milford, MA). Reference compounds, helipyrone, and arzanol (AZL) were obtained following a previously described extraction and purification process from *Helichrysum italicum* subsp. *microphyllum* (Tagliatela-Scafati et al., 2013).

## 2.1.3 | Sample preparation

A portion of 4 mg of HSE was dissolved in 2 mL of MeOH and filtered through a 0.45 µm PTFE filter before the injection into the HPLC system. The sample preparation was performed twice.

## 2.1.4 | Qualitative HPLC-ESI-MS and MS<sup>2</sup> analysis of HSE

The HPLC-ESI-MS<sup>n</sup> analysis of HSE was performed using an Agilent Technologies (Waldbronn, Germany) modular 1200 system, equipped with a vacuum degasser, a binary pump, a thermostated autosampler, a thermostated column compartment, and a 6310A ion trap mass analyzer with an ESI ion source. HPLC analyses were carried out on an Ascentis Express C<sub>18</sub> column (150 mm × 3.0 mm I.D., 2.7 µm, Supelco, Bellefonte, PA), with a mobile phase composed of 0.1% HCOOH in H<sub>2</sub>O (A) and ACN/MeOH (50:50, v/v) (B). The gradient elution was modified as follows: 0–5 min 20% B, 5–10 min from 20% to 50% B, which was kept for 5 min, 15–20 min from 50% to 100% B which was kept for 10 min. The post-running time was 10 min. The flow rate was 0.3 mL/min. The column temperature was set at 30°C. The sample injection volume was 10 µL. The HPLC-ESI-MS<sup>2</sup> system was operated both in the positive and negative ion mode. For the positive ion mode, the experimental parameters were set as follows: the capillary voltage was 3.5 kV, the nebulizer (N<sub>2</sub>) pressure was 32 psi, the drying gas temperature was 350°C, the drying gas flow was 10 L/min, and the skimmer voltage was 40 V. For the negative ion mode, the MS conditions were the same as described above. The mass spectrometer was operated in the full-scan mode in the *m/z* range of 100–1200. MS<sup>2</sup> spectra were automatically performed with helium as the collision gas in the *m/z* range of 100–1500, by using the SmartFrag function, which automatically selects the precursor ion to be fragmented and it eliminates the need for a time-consuming manual collision-induced dissociation (CID) voltage optimization. Data were acquired by Agilent 6300 Series Ion Trap LC/MS system software (version 6.2).

## 2.1.5 | Quantitative HPLC-UV analysis of HSE

The HPLC-UV analysis of HSE was performed on an Agilent Technologies modular model 1260 Infinity II system, consisting of a quaternary pump, a manual injector, and a UV variable wavelength detector. Chromatograms were recorded by using an Agilent OpenLab ChemStation (Rev. C.01.10). The HPLC column and the applied chromatographic conditions were the same as those described for the HPLC-ESI-MS<sup>n</sup> system. Chromatograms were acquired at 280 and 330 nm. Calibration curves for helipyrone and AZL were constructed at five calibration levels in the concentration range 1.8–89.4 mg/mL and 19.8–476.0 mg/mL, respectively, by plotting the peak areas of the analytes vs. their concentration. Three injections were performed for each concentration level. Quantification data are the mean of six results.

## 2.2 | Behavioral studies

### 2.2.1 | Animals

CD1 male mice (2 months) weighting approximately 20 g (Envigo, Varese, Italy) were housed in the Ce.S.A.L. (Centro Stabulazione Animali da Laboratorio, University of Florence) vivarium and used 3 days after their arrival. Mice were housed in standard cages, kept at 23 ± 1°C with a 12 h light/dark cycle, light on at 7 a.m., and fed with standard laboratory diet and tap water ad libitum. All tests were conducted during the light phase. The experimental protocol was approved by the Institution's Animal Care and Research Ethics Committee (University of Florence, Italy), under a license released from the Italian Department of Health (54/2014-B). Mice were treated in accordance with the relevant European Union (Directive 2010/63/EU, the council of 22 September 2010 on the protection of animals used for scientific purposes) and international regulations (Guide for the Care and Use of Laboratory Animals, US National Research Council, 2011). All studies involving animals are reported in accordance with the ARRIVE 2.0 guidelines for experiments involving animals (du Sert et al., 2020). The experimental protocol was designed to minimize the number of animals used and their suffering. The G power software was used to perform a power analysis to choose the number of animals per experiment (Charan & Kantharia, 2013).

### 2.2.2 | Drug administration

Animals were habituated to the experimental room, randomly assigned to each treatment group using simple randomization by an individual other than the operator and investigated by observers blinded for treatment. HSE was dissolved in DMSO, dispersed in 1% carboxymethylcellulose sodium salt (CMC, Fluka Chemie GmbH, Steinheim, Germany) solution to reach the concentration of 1% DMSO, and orally administered for five consecutive days/week for 3 weeks. Control mice received the vehicle (1% DMSO in CMC). HSE was administered at the dose of 100 mg/kg, chosen on the bases of

previous studies (Borgonetti, Les, et al., 2020). Diazepam (DIAZ, 1 mg/kg i.p.) and amitriptyline (AMI, 10 mg/kg i.p.) (Sigma-Aldrich, Milan, Italy) were dissolved in isotonic (NaCl 0.9%) saline solution and administered 30 min before testing. Extracts and drugs were tested as curative treatments.

### 2.2.3 | Evaluation of cumulative food consumption

Mice were tested after 4 h food deprivation with water ad libitum. A weighed amount of standard chow pellets was given to mice and food consumption was evaluated as the difference in weight between that of the initially provided food and that left in the rack, including spillage in the cage. HSE was orally delivered 5 min before food presentation. Cumulative food consumption was measured every 15 min up to 60 min after food presentation on days 1, 7, 14, and 21.

### 2.2.4 | Locomotor activity

*Rotarod test:* The possible onset of motor side effects induced by treatment was evaluated with the rotarod test, as previously described (Galeotti et al., 2006). This test was performed before and on 21 days after the beginning of treatment.

*Hole board test:* The hole-board test is commonly used to verify the effect of a drug on spontaneous mobility and exploratory activity. This test was performed before and 21 days after the beginning of treatment as previously described (Galeotti et al., 2006).

### 2.2.5 | Evaluation of the anxiolytic-like effect

*Open field test (OFT):* This is a test used to assess animal's anxiety-like behavior. A rectangular box (78 × 60 × 39 cm) is used, on which an internal perimeter is traced such as to deviate about 3 cm from the walls. Animals were positioned in the center of the box and then the time each animal remained in the internal portion is measured, over a total duration of 5 min. The longer the animal stays in the center of the arena, the less anxious-like it is (Nogueira Neto et al., 2013). This test was performed before and on days 7, 10, 18, and 21 after the beginning of treatment.

*Light dark box (LDB) test:* The LDB test was performed as previously reported (Borgonetti, Governa, et al., 2020). Briefly, each mouse was allowed to move freely for 5 min in a box with two different compartments, the dark, and the light chamber, separated by a small door (10 cm × 3.2 cm). The time spent in the light was used as a sign of the anxiety state of each animal. This test was performed on day 21 after the beginning of treatment.

### 2.2.6 | Evaluation of the antidepressant activity

*Sucrose splash test (SST):* A 10% sucrose solution in H<sub>2</sub>O is prepared and a small amount of this is placed on the animal's back. The mouse

is placed inside a box and the time spent cleaning in 5 min is measured. The purpose is to obtain information about the state of depressive-like behavior of the mouse. In fact, the more this will be marked, the more difficult the animal will tend to clean itself (Borgonetti & Galeotti, 2022). This test was performed before and on days 7, 10, 18, and 21 after the beginning of treatment.

*Tail suspension test (TST):* Mice were suspended from a pole mounted 50 cm above the floor using adhesive tape placed in the middle of the tail. The time during which the mice remained immobile was measured with a stopwatch during a 6-min test period. Mice were considered immobile when they hung passively and completely still, except for movements caused by breathing. Immobility was considered a depression-like behavior (behavioral despair) and was measured in the first 2 min of the test, when the animals are reacting to unavoidable stress and is a measure of the basal level of depression, and in the last 4 min, when behavioral despair is established (Borgonetti, Les, et al., 2020). This test was performed on day 21 after surgery.

### 2.2.7 | Evaluation of mnemonic functions

*Novel Object Recognition Test (NORT):* The test was performed in an arena in which the animal was allowed to move freely, as previously described (Galeotti et al., 2013). Briefly, in the acclimatization session, no objects were placed in the box. In the first session (Day 1-training session), animals were placed in the center of the arena and presented with two identical objects (A1 and A2). Exploration time assessed as sniffing or touching the object with the nose and mouth was recorded. Two different operators recorded the time of the animal on each object. To measure long-term memory, animals were placed back in the same arena 24 h after (Day 2-retention session) with two objects, the familiar A1 (the same as the day before) and a new object B for 5 min. Objects A1 and B had different shapes, colors, and sizes that had no meaning for the animals. The objects and apparatus were cleaned with an ethanol solution between tests to remove olfactory cues.

It was recorded: (i) time spent by the animals observing the two objects A1 and A2, (ii) the difference in discrimination between object A1 and object B, (iii) the percentage of time spent by each animal in exploring the object A1 between the training and the retention session calculated as: TA1x100/5 min. This test was performed on day 21 after the beginning of treatment.

## 2.3 | Cell culture studies

### 2.3.1 | Model of excitotoxicity in cell culture

A human neuroblastoma cell line (SH-SY5Y, passages 6–20, Cat# 94,030,304 ECACC), was cultured in DMEM (Merck, Darmstadt, Germany) and F12 Ham's nutrients mixture (Merck), containing 10% heat-inactivated FBS (Merck), 1% L-glutamine (Merck), and 1% penicillin–streptomycin solution (Merck) until confluence (70%–80%).

The cells were grown in a humidified atmosphere with 5% CO<sub>2</sub> at 37°C. EDTA-trypsin solution (Merck) was used for detaching the cells from flasks, and cell counting was performed using a hemocytometer by Trypan blue staining.

L-glutamate (GLU, Merck) was used to induce the excitotoxic stimulation of SH-SY5Y cells (Kritis et al., 2015). A 800 mM stock solution of monosodium glutamate (Sigma-Aldrich) was prepared in sterile DMEM. Later, it was filtered and diluted in a complete medium for the cell treatments. HSE (0.1–100 µg/mL) and arzanol (AZL, Merck) were dissolved in DMSO making a stock of 10 mg/mL, and then diluted for reaching the concentration in the DMEM/F12 with a low concentration of FBS (3%). The SH-SY5Y cells were pre-treated for 4 h with HSE or AZL and then stimulated with glutamate 80 mM for 24 h (Borgonetti, Les, et al., 2020).

### 2.3.2 | CCK-8 test

Cell viability was performed using a Cell Counting Kit (CCK-8, Merck) according to the manufacturer's instructions. A total of  $5.0 \times 10^5$  cells/well were seeded into 96 multi-well plates and grown to confluence. The absorbance was measured at 450 nm using a microplate photometer HiPo MPP-96 (Biosan, Riga, Latvia). The treatments were performed in six replicates in three independent experiments, and the cell viability was calculated by normalizing the values to the control's mean (Borgonetti et al., 2022).

### 2.3.3 | Sulforhodamine B assay

Cells ( $5 \times 10^5$  cells in 200 mL) were seeded in 96-well plates to perform this experiment. Briefly, after treatments with HSE and AZL, serum-free medium containing trichloroacetic acid (TCA 500 mg/mL) was added to cells. The plate was then incubated at 4°C for 1 h. Wells were then washed 5 times with double distilled water and left overnight to dry at room temperature (rt). The next day, 30 mL of a 4 mg/mL SRB solution in 1% acetic acid was added to each well and incubated for 30 min at rt, followed by 4–5 washes with 1% acetic acid, and, finally, added with a Tris-HCL solution (pH 10) for each well and incubated for 5 min with shaking. The absorbance was read at a wavelength of 570 nm using a microplate photometer HiPo MPP-96 (Biosan). The treatments were performed in six replicates in three independent experiments, and cell viability was calculated by normalizing the values to the control's mean (Borgonetti & Galeotti, 2022).

## 2.4 | Preparation of tissue and cell lysates, western blot, and immunofluorescence

The detailed protocols used for preparing tissue and cell lysates and for performing SIRT1 enzymatic assay, western blot and immunofluorescence are described in [Supporting Information](#).

### 2.4.1 | Computational analysis

The crystal structure of SIRT1 in complex with the 4-(4-{2-[(methylsulfonyl)amino]ethyl}piperidin-1-yl) thieno [3,2-d] pyrimidine-6-carboxamide inhibitor (PDBID: 4zzi; resolution: 2.73 Å) was prepared using the Protein Preparation Wizard available in Maestro (Schrodinger software suite, release 2019-02) to assign bond orders, add hydrogen atoms, adjust missing side chains, cap termini, and generate tautomeric states. The 2D structures of HSE constituents were retrieved from PubChem and converted to 3D using the LigPrep routine (Schrodinger) generating possible ionization and tautomeric states. All ligands and protein were converted to PDBQT format using OpenBabel (O'Boyle et al., 2011) and molecular docking was performed using AutoDock Vina (Trott & Olson, 2009). The protein was treated as rigid, and the grid box was centered on the co-crystallized ligands (box center: x: −11.638, y: 61.009, z: 5.53) and sized to be 20 × 20 × 20 Å. Exhaustiveness was set to 24.

### 2.5 | Statistical analysis

Results are expressed as mean ± SEM. One-way and Two-way analysis of variance (ANOVA), followed by Bonferroni or Tukey post-hoc test, respectively, were used for behavioral tests. ANOVA followed by specific post-hoc was used for statistical analysis of in vitro data ( $n = 6$ ). Student t-test was used when necessary. For each test, a value of  $p < 0.05$  was considered significant. The software GraphPad Prism version 9.1.2 (GraphPad Software, San Diego, CA) was used in all statistical analyses.

## 3 | RESULTS

### 3.1 | Chemical characterization of HSE

The compounds identified in HSE, together with their acquired spectral data, are shown in Table S1. A representative HPLC-UV chromatogram of the extract, acquired at 280 nm, is shown in Figure 1. All the compounds listed in Table S1 were identified by comparing chromatographic, MS, and MS<sup>2</sup> data with those described in the literature for the same compounds and matrix. The only exception was represented by helipyron and AZL, whose identity was confirmed also using the reference isolated compounds.

Compounds 1 and 31 ionized better in the positive ion mode and, therefore, their identification was based on their fragmentation in this polarity. In particular, compound 1 with a  $[M+H]^+ = 381$  was identified as bitalin A12-glucoside, since it showed a product ion at  $m/z$  219, generated by the loss of a hexoside group (Judzentiene et al., 2022). Compound 31 with a  $[M+H]^+ = 345$  was identified as 3,5-dihydroxy-6,7,8-trimethoxyflavone, since it generated two product ions at  $m/z$  330 and 315, corresponding to the loss of two methyl groups (Les et al., 2017).



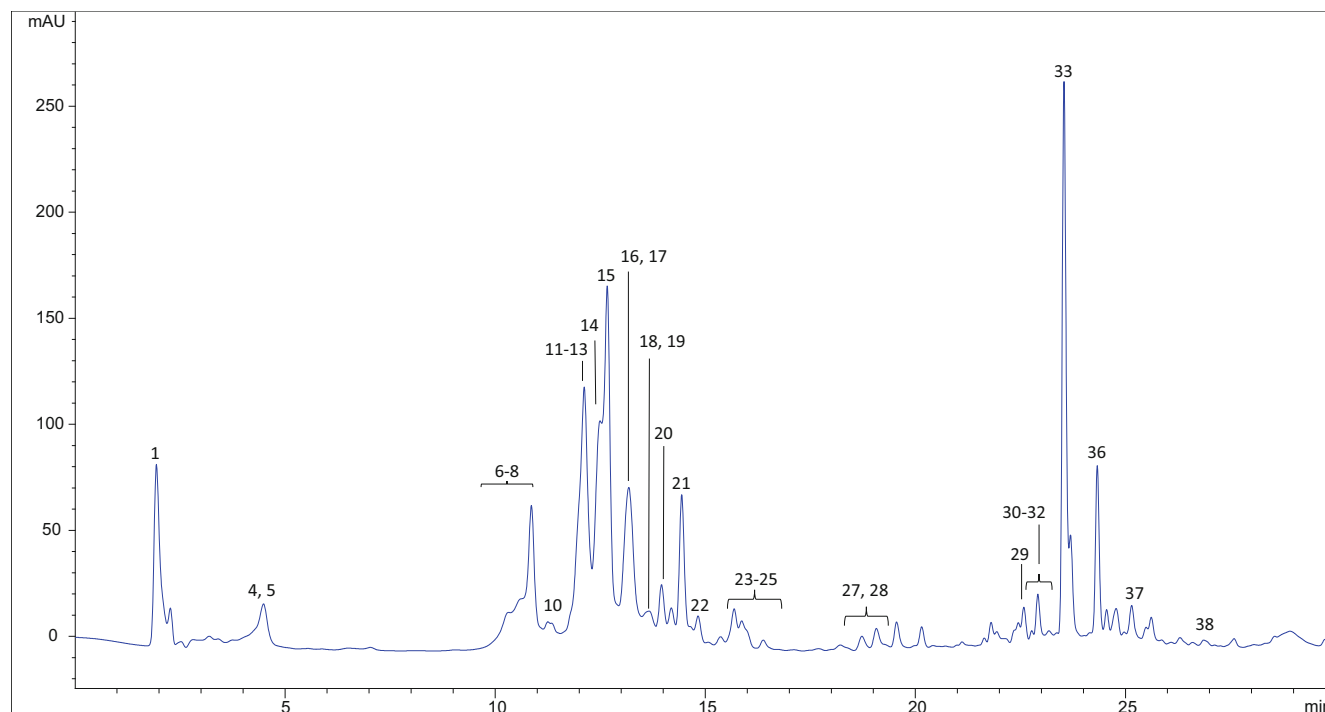


**FIGURE 1** HPLC-UV chromatogram of the *Helichrysum stoechas* extract (HSE), acquired at 280 nm. For peak assignment, see Table S1.

All the other identified compounds in HSE showed better fragmentation when the mass analyzer was operated in the negative ion mode. Therefore, further discussion on their identification is based only on these data. Compound **2**, having a  $[M-H]^- = 315$ , showed a product ion at  $m/z$  153, corresponding to the loss of a hexoside group ( $-162$  Da), but it also showed an additional product ion at  $m/z$  109, generated by the subsequent loss of a carboxylic group ( $-44$  Da). So, it was identified as protocatechuic acid O-hexoside (Kramberger et al., 2020).

Compounds **3–5**, having a  $[M-H]^- = 353$ , were identified as caffeoylquinic acid isomers, since they presented the typical fragmentation pattern widely described in the literature for these compounds (Kramberger et al., 2020; Vujić et al., 2020).

Compounds **6–9** with a  $[M-H]^- = 479$  showed a product ion at  $m/z$  317, corresponding to the aglycon myricetin. So, they were identified as myricetin glycoside isomers (Kramberger et al., 2020).

Compounds **10–12**, **14**, and **20** with a  $[M-H]^- = 463$  showed a product ion at  $m/z$  301, corresponding to quercetin. For this reason, they were identified as quercetin hexoside isomers (Kramberger et al., 2020; Vujić et al., 2020).

Compound **13**, having a  $[M-H]^- = 565$ , was identified as myricetin malonyl hexoside, since it showed a product ion at  $m/z$  521, corresponding to the loss of a carboxylic group, together with an additional fragment at  $m/z$  317, corresponding to myricetin (Kramberger et al., 2020).

Compounds **15**, **16**, and **18** with a  $[M-H]^- = 515$  showed a similar fragmentation pattern with the presence of a product ion at  $m/z$  353, corresponding to the loss of a hexoside group. They were identified as dicaffeoyl quinic acid isomers, according to the literature (Kramberger et al., 2020; Vujić et al., 2020).

Compounds **17** and **19** with a  $[M-H]^- = 477$  were identified as isorhamnetin hexoside isomers, since they showed a product ion at  $m/z$  315, corresponding to isorhamnetin (Kramberger et al., 2020).

Compounds **21**, **22**, and **26**, having a  $[M-H]^- = 609$ , showed a main product ion at  $m/z$  463 and at  $m/z$  301, resulting from the loss of a coumaroyl and a coumaroyl hexoside moiety, respectively. This allowed us to tentatively identify these compounds as quercetin-coumaroyl-glucoside isomers, since the fragment at  $m/z$  301 corresponds to quercetin (Kramberger et al., 2020).

Compounds **23** and **25** both with a  $[M-H]^- = 593$  showed a product ion at  $m/z$  285, corresponding to the loss of a coumaroyl group, followed by the loss of a hexose group, which corresponds to kaempferol. These compounds were identified as tilioside isomers (kaempferol-coumaroyl-glucoside) (Kramberger et al., 2020; Vujić et al., 2020).

Compound **24**, showing a  $[M-H]^- = 301$ , possesses the fragmentation pattern already described in the literature for quercetin (Kramberger et al., 2020; Vujić et al., 2020).

Compounds **27** and **28**, having a  $[M-H]^- = 269$  and  $285$ , respectively, were identified as apigenin and kaempferol, since they presented a fragmentation pattern compliant with what described in the literature for these compounds (Cerrato et al., 2020; Gouveia & Castilho, 2010; Judzentiene et al., 2022).

Compound **29** with a  $[M-H]^- = 359$  showed two product ions at  $m/z$  344 and  $m/z$  329, corresponding to two subsequent losses of a methyl group. This fragmentation pattern was described in the literature for two compounds, which were tentatively identified as myricetin-3,3',4'-trimethyl-ether and methoxyquercetin-dimethyl-ether (Méndez et al., 2021).

Compound **30**, having a  $[M-H]^- = 313$ , and compound **32**, having  $[M-H]^- = 283$ , respectively, were identified as gnaphaliin and galangin-methyl-ether, given their fragmentation pattern compliant with the literature (Kramberger et al., 2020).

Compounds **33** with a  $[M-H]^- = 359$ , **34**, and **37** with a  $[M-H]^- = 373$  showed a similar fragmentation pattern, with a main product ion at  $m/z$  207. This fragment is typical of type I homoisoflavonoids, resulting from the  $C_{3-9}$  bond cleavage (Ye et al., 2005). Compound **34** was tentatively identified as 5,7,4'-trihydroxy-3',5'-dimethoxy-6,8-dimethyl homoisoflavanone, and compound **37** as its isomer, respectively. Compound **33** showed the same fragmentation pattern, but a different mass; so it was tentatively identified as 5,7,3',5'-tetrahydroxy-4'-methoxy-6,8-dimethyl homoisoflavanone (Ye et al., 2005). To the best of our knowledge, this is the first time that this chemical class of molecules is described in *H. stoechas*.

Compound **35**, having a  $[M-H]^- = 375$ , was identified as a dihydroxydimethoxy flavone derivative, since its fragmentation pattern was coherent with what has already been described in the literature (Gouveia & Castilho, 2010).

Compound **36** with a  $[M-H]^- = 319$  was identified as helipyronone as its fragmentation pattern and its presence in *Helichrysum* species has been well documented in the literature (Kramberger et al., 2020). In addition, its identity was confirmed also using the pure compound isolated from the plant (Taglialatela-Scafati et al., 2013).

Compound **38**, having a  $[M-H]^- = 401$ , was identified as arzanol, which is another typical compound found in *Helichrysum* species (Kramberger et al., 2020; Vujić et al., 2020). Its identity was also confirmed with the pure compound isolated from the plant (Taglialatela-Scafati et al., 2013).

Compounds **39** and **41** with a  $[M-H]^- = 399$  were identified as italipyronone 1 and 2 (Kramberger et al., 2020). Compounds **40** and **42-44** with a  $[M-H]^- = 415$  were identified as methylarzanol isomers (Kramberger et al., 2020). Compound **45** with a  $[M-H]^- = 415$  was identified as heliarzanol (Kramberger et al., 2020). All these compounds showed a fragmentation pattern compliant with that described in the literature for this class of compounds and their presence has already been described in *H. stoechas* (Kramberger et al., 2020).

### 3.2 | Quantitative analysis of peculiar compounds in HSE

HSE was found to be remarkably rich in polyphenols, with a total content of  $201.7 \pm 26.1$  mg<sub>gallic acid equivalents</sub>/g, as determined using the Folin-Ciocalteu's spectrophotometric method (Filaferro et al., 2022), which agrees with what has been previously described in the literature for the same extract ( $166.6 \pm 20.1$  mg GAE/g) (Les et al., 2017).

The total flavonoid content of HSE was  $75.8 \pm 9.1$  mg<sub>quercetin equivalents</sub>/g, as determined through aluminium chloride spectrophotometric method (Filaferro et al., 2022).

Helipyronone and AZL, which are typical compounds from *Helichrysum* species (Kramberger et al., 2020; Les et al., 2017; Taglialatela-

Scafati et al., 2013), were quantified using HPLC-UV and their amount was  $4.7 \pm 0.4$  mg/g and  $41.1 \pm 3.4$  mg/g, respectively. AZL quantitative data are compliant with what has already been described in the literature for the dried plant material (Kramberger et al., 2020).

### 3.3 | HSE reduced animal body weight

The mouse body weight was evaluated before treatment and monitored daily after HSE oral administration for 21 days (Figure 2a). Control mice (CTRL) showed a progressive and constant increase in body weight. HSE-treated mice showed a trend to weight gain, but of much lower intensity than CTRL over the whole duration of the test. The difference in body weights between groups became significant starting from the second week of treatment and persisted after 3 weeks (Figure 2b). By comparing the mouse body weight before the beginning of the test (BL) with that reached on day 21, we observed a significant weight gain in CTRL as expected. Conversely, the increase in body weight in the HSE group did not reach statistical significance showing values comparable to that recorded before the beginning of the test (Figure 2c).

To study the mechanism involved in the control of weight gain by HSE, we first investigated whether the extract could exert an anorexic effect. The cumulative food consumption was evaluated after acute administration of HSE in mice deprived of food for 4 h. A reduction in food eaten was observed after 15 min that reached statistical significance after 30 min. The effect of HSE was short-lived as no difference in food consumption was observed between the control and the treated groups 60 min after the injection (Figure 2d). Then, the daily food consumption during HSE repeated administration was evaluated. Even though a trend toward a hypophagic effect was observed, no significant difference was detected at any time point in comparison with the CTRL group (Figure 2e). These results indicated that, even though a short-lasting reduction of food consumption was observed after acute administration, HSE did not prominently act as anorexic agent.

### 3.4 | Anxiolytic-like and antidepressant-like activity of HSE

To evaluate if HSE, at the dose effective in reducing body weight, was able to modulate the response to exposure to an anxiety-related environment, the open field test (OFT) and light-dark box (LDB) tests were performed (Figure 3a). In the OFT, repeated administration of HSE 100 mg/kg p.o. increased the time spent in the center, defined as a parameter of anxiolytic-like activity. This effect was significant after 7 days of treatment and remained unaltered up to the end of the experimentation (day 21), indicating the lack of induction of tolerance by the extract (Figure 3b). To further confirm and extend these data, the effect of HSE was evaluated in the LDB test. The effect of repeatedly administered HSE was detected on day 21 and the efficacy was compared to that of HSE acutely delivered as a single administration. Acute HSE prolonged the time spent in the light chamber, producing

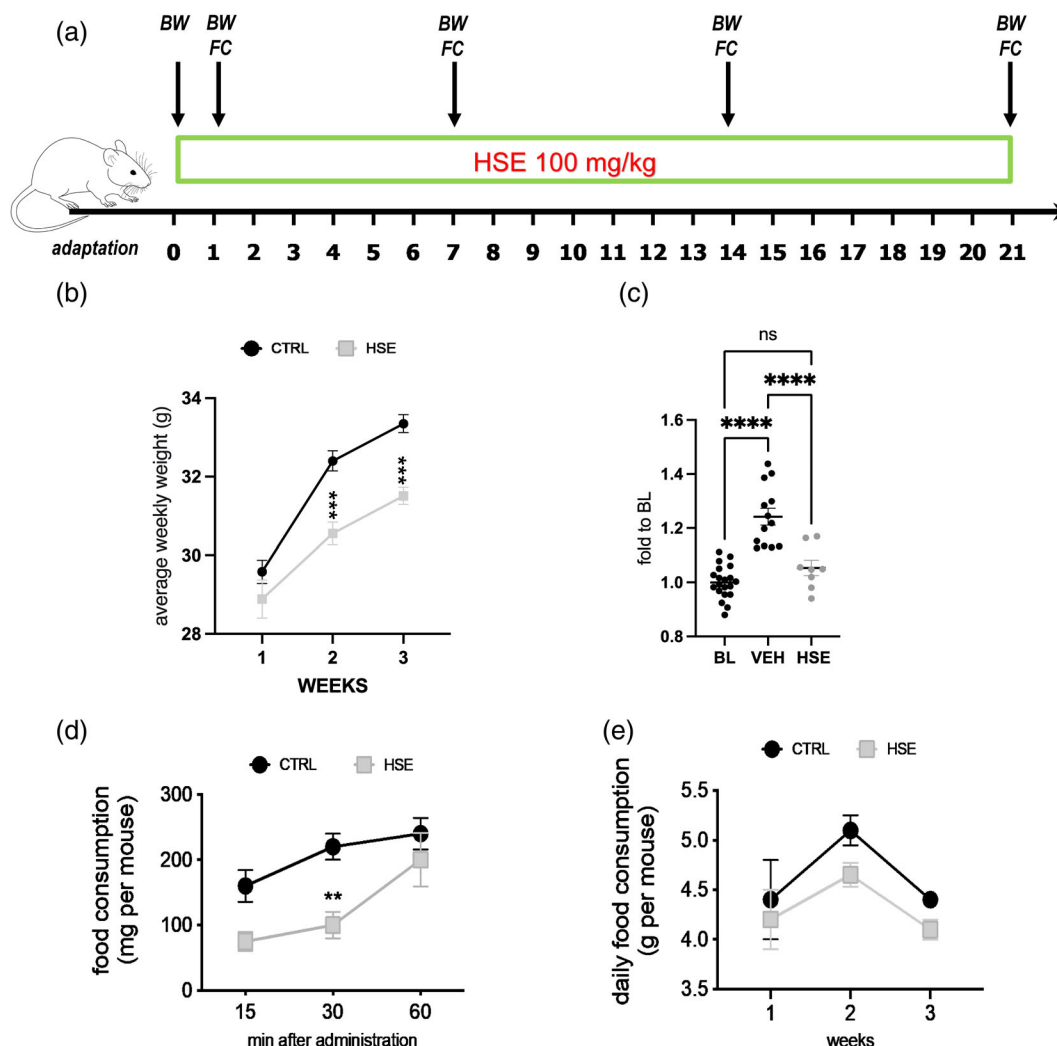


**FIGURE 2** HSE reduction of body weight. (a) Schematic representation of the experimental protocol. BW, body weight; FC, food consumption. (b) HSE (100 mg/kg) repeated administration reduced the body weight gain over the 3 weeks period of experimentation in comparison with control (CTRL) mice. \*\*\* $p < 0.001$  vs. CTRL. (c) Comparison of the mouse body weight before the beginning of the test (BL) with that reached on day 21 by CTRL and HSE-treated mice. \*\*\*\* $p < 0.0001$ ; ns: not significant. (d) The cumulative food consumption was evaluated after acute administration of HSE in mice deprived of food for 4 h, compared to the CTRL group. \*\* $p < 0.01$  vs. CTRL. (e) Daily food consumption during HSE repeated administration. Values were recorded on days 7, 14, and 21 from the beginning of the test. Eight mice per group were used.

an anxiolytic-like effect comparable to that induced by diazepam (DIAZ) 1 mg/kg, used as a reference drug. Following repeated treatment, HSE more markedly increased the time spent in the light compartment with an anxiolytic-like effect that was significantly higher than that of DIAZ (Figure 3c). In these experimental conditions, a second behavioral parameter detected to evaluate the anxiolytic efficacy of the treatment was the number of transitions between the two chambers. Results revealed that acute HSE, compared to repeated HSE, showed a higher increase in the number of transitions (Figure 3d).

The sucrose splash test (SST) and the tail suspension test (TST) were performed to assess the antidepressant-like activity of HSE. The evaluation of the time spent in grooming behavior in the SST showed comparable results in both CTRL and HSE-treated groups up to 18 days of treatment. On day 21 the grooming behavior in HSE-treated mice was drastically increased, indicating the induction of an antidepressant-like

behavior (Figure 3e). To further corroborate these results, the TST was performed. In the first 2 min of the test, when the behavioral despair is not yet established, no effect by treatment was observed (Figure 3f). In the last 4 min of the experimental procedure, a depressive-like behavior develops as a response to short-term, unavoidable stress of being suspended by their tail that is detected as immobility time. Repeated HSE administration reduced the immobility time with comparable intensity to amitriptyline, used as an antidepressant reference drug. Conversely, acute HSE injection did not produce any effect (Figure 3g).

### 3.5 | Neuroprotective effect of HSE on SH-SY5Y

Silent information regulator 1 (SIRT1) is expressed in both neurons and glial cells (Chen et al., 2005; Hisahara et al., 2008). To assess the



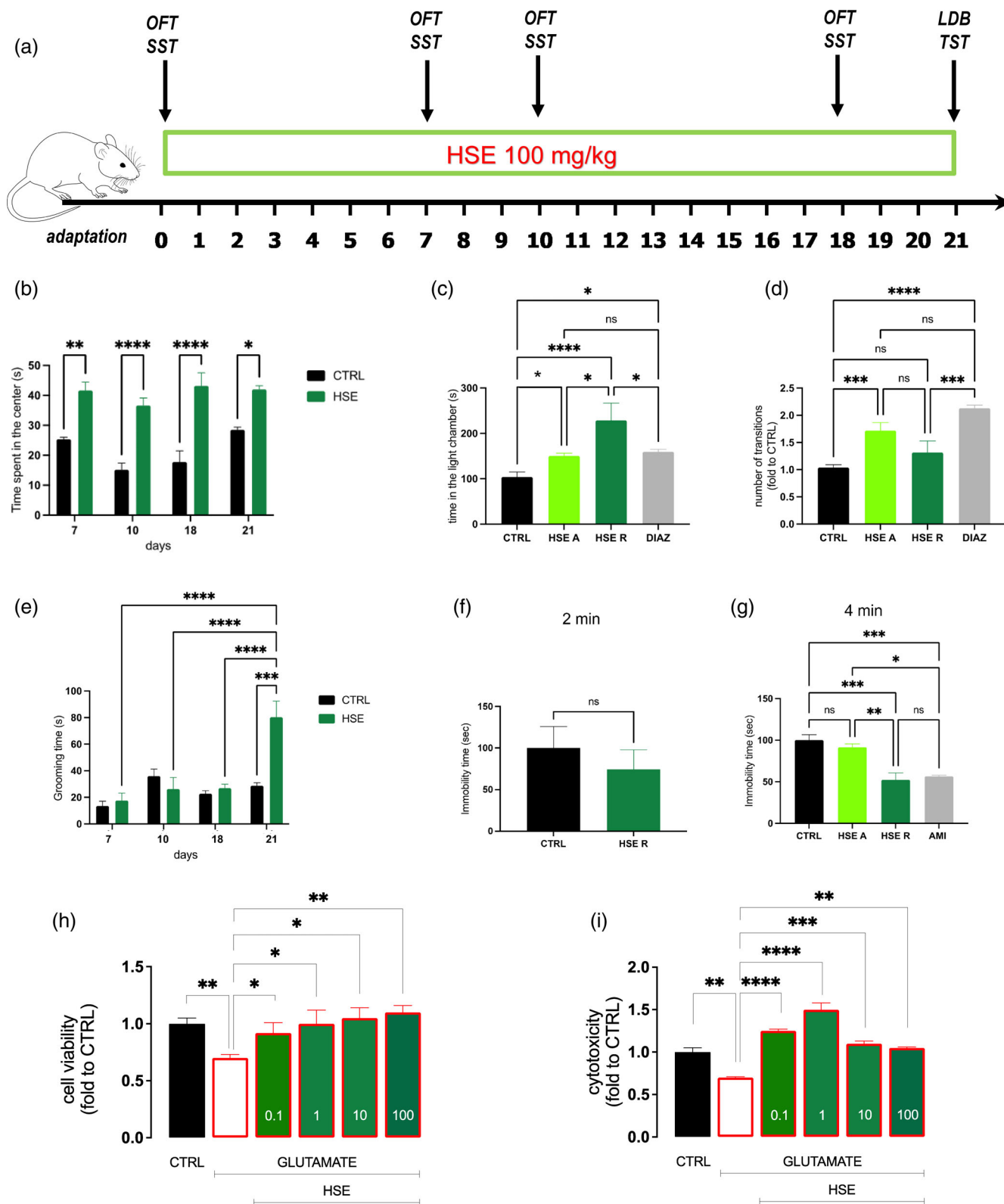


**FIGURE 3** Legend on next page.

neuronal mechanism in the HSE effects, the induction of a potential neuroprotective activity was evaluated by reproducing a model of excitotoxicity induced by an overload of glutamate in SH-SY5Y human neuroblastoma cell line. SH-SY5Y neuronal cells were stimulated with

glutamate for 24 h and a significant reduction of cell viability was induced. Pretreatment of cells for 4 h with HSE (0.1–100  $\mu$ M) before the glutamate stimulation counteracted the excitotoxic effect by completely preventing the reduction in cell viability in the CCK-8

test (Figure 3h). HSE pretreatment (0.1–100 µg/mL) also reduced cytotoxicity in the SRB test (Figure 3i).

### 3.6 | Effect of HSE on SIRT1-FoxO1 pathway

SIRT1 belongs to the sirtuins (the class III of histone deacetylases) and it is generally considered a hypothalamic energy sensor (Imai et al., 2000). SIRT1, which is expressed in proopiomelanocortin (POMC)- and agouti-related peptides (AgRP)-neurons within the hypothalamic arcuate nucleus and mainly via its deacetylation of Forkhead Box O1 transcription factor (FoxO1), positively regulates AgRP transcription (increase food intake) while it negatively regulates POMC (satiety) (Sasaki & Kitamura, 2010).

Glutamate exposure of SH-SY5Y cells was related to the overexpression of SIRT1. Western Blot (WB) experiments showed a SIRT1 increase of about 1.5-fold to CTRL. This effect was partially reduced by pretreatment with HSE 0.1 µg/mL, while doses from 1 to 100 µg/mL reduced the SIRT1 protein content in a dose-dependent manner up to approximately 50% of CTRL levels (Figure 4a). Immunofluorescence (IF) images illustrated the increased SIRT1 immunostaining in SH-SY5Y cells that was robustly decreased by HSE treatment (Figure 4b). Quantitative analysis of SIRT1 protein levels confirmed the drastic reduction of the protein content (Figure 4c).

In the CNS, SIRT1 is prominently expressed in the hypothalamus and hippocampus (Ramadori et al., 2008). Evidence shows that SIRT1 requires FoxO1 to control hypothalamic functions (Cyr et al., 2015). To correlate the modulation of the SIRT1-FoxO1 pathway to the modulation of feeding behavior by treatment, we investigated whether an inhibitory effect on the FoxO1 pathway by repeated HSE occurred in the mouse hypothalamus. IF experiments showed a lower FoxO1 immunostaining in the HSE-treated group in comparison with CTRL (Figure 4d). Quantitative analysis of fluorescence confirmed the significant reduction of FoxO1 protein expression (Figure 4e).

Due to the well-known bidirectional association between mood alteration and weight gain, we investigated whether hippocampal SIRT1 expression might be modulated by HSE. WB experiments showed a robust increase in the expression of the SIRT1 protein in the hippocampus of CTRL mice exposed to a stressful environment in the LDB test in comparison with naïve mice. HSE treatment

drastically reduced hippocampal SIRT1 expression to values recorded in naïve mice (Figure 5f). Triple staining IF experiments showed the expression of SIRT1 in NeuN-positive cells, indicating the neuronal localization of hippocampal SIRT1. Consistent with WB results, a drastic reduction in SIRT1 expression following HSE repeated administration was shown by IF images (Figure 4g) and confirmed by quantification analysis (Figure 4h).

### 3.7 | SIRT1 inhibitory activity and molecular modeling

Findings on the capability of HSE to attenuate SIRT1 signaling encouraged us to perform further experiments to evaluate its capacity to act as a SIRT1 inhibitor and to identify the main constituent (s) that might be responsible for this activity.

First, we performed molecular docking simulations of the constituents identified in HSE in the SIRT1 inhibitor binding site. The redocking simulation of the 4-(4-{2-[(methylsulfonyl)amino]ethyl} piperidin-1-yl) thieno [3,2-d]pyrimidine-6-carboxamide inhibitor confirmed the reliability of AutoDock Vina in predicting the binding mode of the co-crystallized ligand in the active site of SIRT-1 (RMSD = 0.745 Å). After a careful evaluation of the docking pose, AZL (Vina binding energy: −9.0 kcal/mol) was selected as the most promising candidate for SIRT1 inhibition. Indeed, AZL fits very well within the binding site occupied by the co-crystallized inhibitor, with four hydrogen bonds (with Arg274, Tyr280, Gln345, and Ile347), representing the major anchor points for its binding (Figure 5b).

To confirm the docking results, we evaluated the inhibitory activity of HSE on SIRT1 activity in vitro, using an enzymatic assay. HSE showed inhibitory effects on SIRT1 enzymatic activity with an IC<sub>50</sub> of 0.25 µg/mL (Figure 5c). Next, we tested the inhibitory activity of AZL in comparison with nicotinamide, used as reference drug. The results from the enzymatic assay showed comparable SIRT1 inhibition between AZL and nicotinamide at 10 and 100 µM, with AZL being even more active than the reference compound at 100 µM (Figure 5d).

To finally correlate computational analysis and enzymatic activity with biological effects, we tested AZL on glutamate-stimulated SH-SY5Y cells. IF experiments showed a reduced SIRT1 immunostaining following AZL treatment (Figure 5e), confirmed by quantification analysis (Figure 5f). The effect of AZL was comparable to that of HSE

**FIGURE 3** HSE induced anxiolytic-like and antidepressant-like effects. (a) Schematic representation of the experimental protocol. LDB, light dark box; OFT, open field test; SST, sucrose splash test; TST, tail suspension test. (b) Repeated administration of HSE 100 mg/kg p.o. increased the time spent in the center in the OF test starting from 7 days of treatment. (c) Acute HSE administration prolonged the time spent in the light chamber in the LDB test. A more pronounced effect was obtained following repeated administration (test on day 21). Diazepam (1 mg/kg i.p.) was used as a reference drug. \* $p < 0.05$ ; \*\*\*\* $p < 0.0001$ ; ns: not significant. (d) Evaluation of the number of transitions between the two chambers in the LDB test. Diazepam (1 mg/kg i.p.) was used as a reference drug. \*\*\* $p < 0.001$ ; \*\*\*\* $p < 0.0001$ ; ns: not significant. (e) Increase in the time spent in grooming behavior in the SST by HSE repeated treatment after 21 days of treatment. \*\*\* $p < 0.001$ ; \*\*\*\* $p < 0.0001$ . (f, g) Decrease of the immobility time in the TSS by HSE repeated administration in the last 4-min period of the test and lack of activity by acute administration. Amitriptyline (10 mg/kg i.p.) was used as a reference drug. \* $p < 0.05$ ; \*\*\* $p < 0.001$ ; ns: not significant. For all behavioral tests, height mice per group were used. (h, i) Neuroprotective effect of HSE (0.1–100 µg/mL) on glutamate-stimulated SH-SY5Y cells evaluated as prevention of the reduction in cell viability in the CCK-8 test and reduced cytotoxicity in the SRB test. \* $p < 0.05$ ; \*\* $p < 0.01$ ; \*\*\* $p < 0.001$ ; \*\*\*\* $p < 0.0001$ .

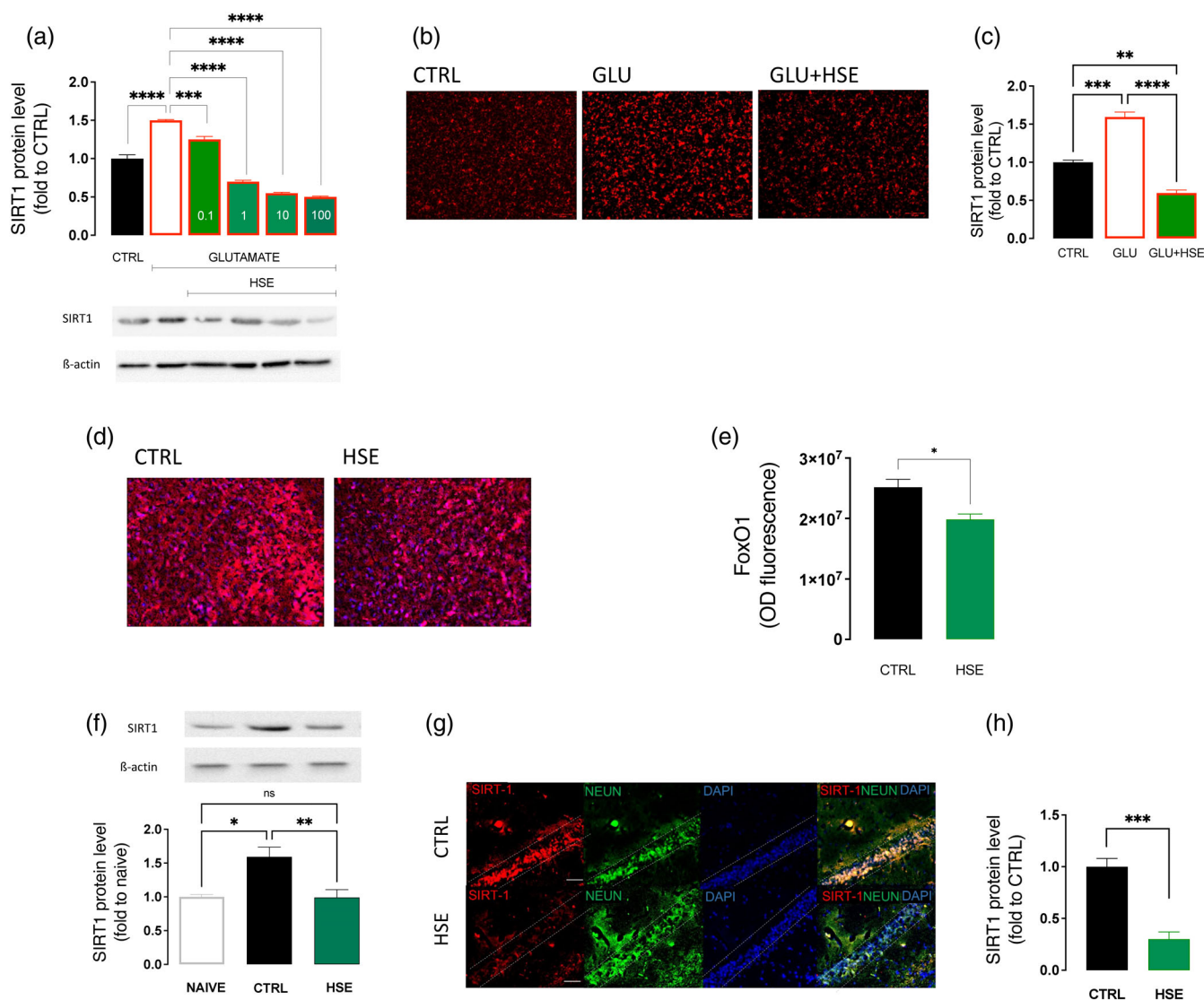


**FIGURE 4** Effect of HSE on SIRT1-FoxO1 signaling pathway. (a) Western Blotting experiments showed a dose-dependent reversal of the overexpression of SIRT1 in glutamate-exposed SH-SY5Y cells by HSE (0.1–100  $\mu$ g/mL). \*\*\* $p$  < 0.001; \*\*\*\* $p$  < 0.0001. (b) Immunofluorescence and (c) quantification analysis illustrated the increased staining of SIRT1 in SH-SY5Y cells that was decreased by HSE (100  $\mu$ g/mL). \*\* $p$  < 0.01; \*\*\* $p$  < 0.001; \*\*\*\* $p$  < 0.0001. (d) Decrease of FoxO1 immunostaining in hypothalamus samples from HSE-treated mice in comparison with the control group (CTRL). (e) Fluorescence quantification analysis of hypothalamic slice staining. \* $p$  < 0.05. (f) Increased expression of SIRT1 protein in the hippocampus of CTRL mice exposed to a stressful environment in the LDB test in comparison with naïve mice. SIRT1 reduction by HSE treatment. Representative blots are reported. \* $p$  < 0.05; \*\* $p$  < 0.01; ns: not significant. (g) Triple staining IF on hippocampal slices showed the expression of SIRT1 in NeuN-positive cells and the reduction of SIRT1 immunostaining by HSE treatment, confirmed by (h) quantification analysis. Western blotting: five mice per treatment group were used and each run was in triplicate. Immunofluorescence: Immunoreactive areas are mean values of five separate experiments. Individual experiments consisted of five tissue sections of each of the six animals per group.

(Figure 4c), confirming this compound as the responsible for the SIRT1 inhibitory activity of HSE.

### 3.8 | Lack of locomotor and mnemonic side effects by HSE

Repeated administration of HSE for 3 weeks did not show any visible sign of sedation or alteration of animal gross behavior. In addition, specific tests to evaluate the locomotor behavior were

performed (Figure 6a). HSE repeated treatment did not alter the spontaneous mobility and the exploratory activity (Figure 6b), evaluated by the hole board test, nor modified the motor coordination in the rotarod test (Figure 6c). In addition to emotions, SIRT1 has been reported to mediate other high-order brain functions, including learning and memory (Fagerli et al., 2022). To exclude any memory impairment by HSE treatment, the novel object recognition test (NORT) was performed. No difference was detected between values recorded from mice treated with HSE at the dose effective on reducing body weight, and CTRL group as indicated by

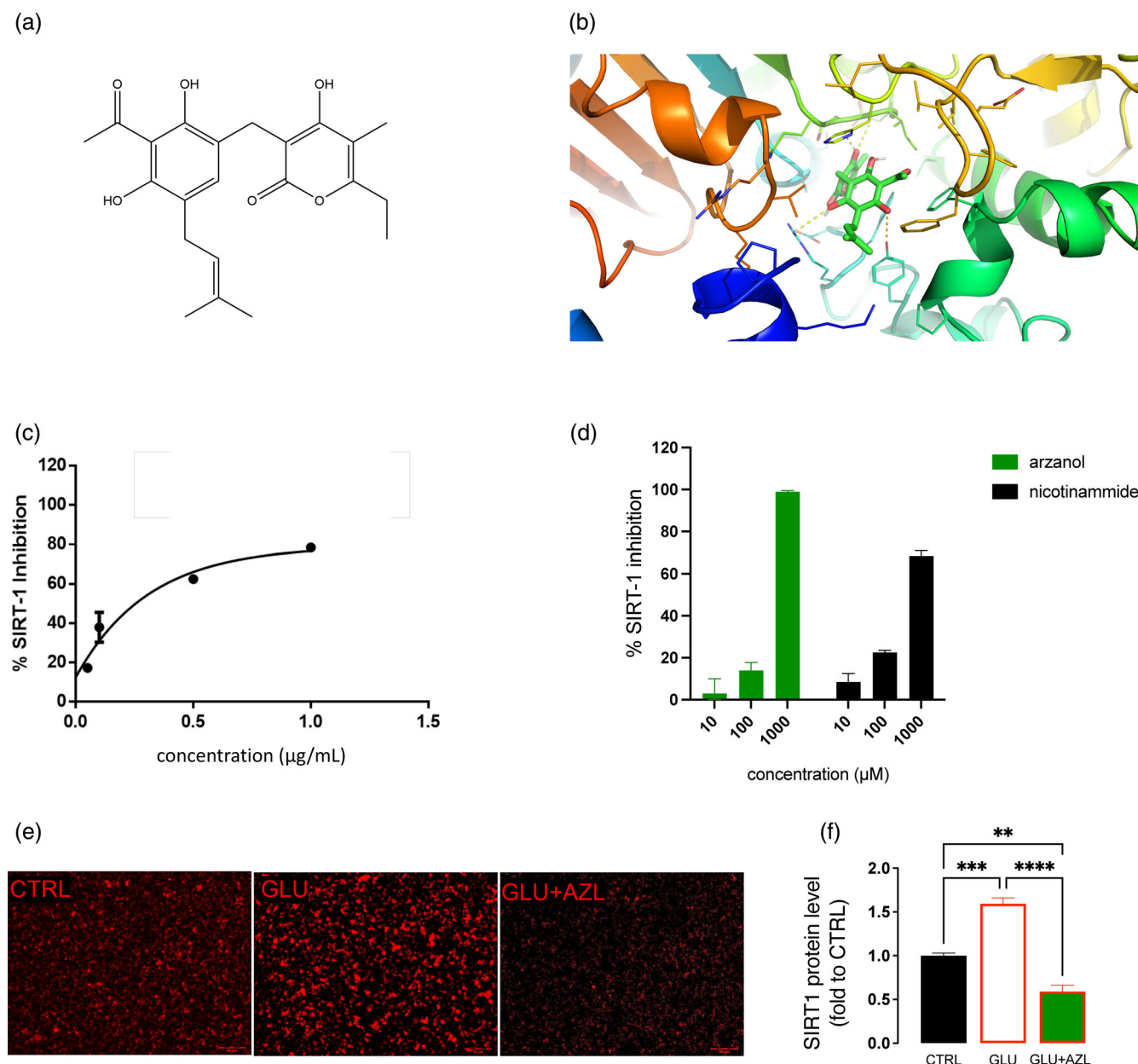


**FIGURE 5** HSE and AZL act as SIRT1 inhibitors. (a) 2D chemical structure of AZL. (b) Binding pose of AZL (green sticks) in the active site of SIRT-1 (PDBID: 4zzi). Residues interacting with the ligand are shown as lines, while hydrogen bonds are shown as yellow dashed lines. Evaluation of the in vitro inhibitory activity of (c) HSE and (d) AZL on SIRT1. Nicotinamide was used as a reference drug. Reduction of SIRT1 (e) immunostaining and (f) protein expression by AZL on glutamate-stimulated (GLU) SH-SY5Y, compared to control (CTRL). \*\* $p < 0.01$ ; \*\*\* $p < 0.001$ ; \*\*\*\* $p < 0.0001$ .

comparable values of inspection activity recorded in the retention session (Figure 6d) and by similar recognition index (Figure 6e) and discrimination index (Figure 6f).

## 4 | DISCUSSION

In the last decades, the number of overweight and obese subjects is dramatically rising. Obesity impacts the functionality of many organs and tissues, representing a major health problem (Williams et al., 2015).

Increasing evidence associates obesity with neurological disturbances, including mood disorders (Milaneschi et al., 2019; Williams et al., 2015). Available drugs, even if effective, have often important safety concerns (Patel & Stanford, 2018). Thus, treatments able to reduce body weight and control depression and anxiety endowed with a favorable safety profile could represent an improvement on current therapies.

In the effort for searching new natural interventions for body weight management, in the present study, we investigated the pharmacological profile of a methanolic extract of *Helichrysum stoechas* (L.) Moench (HSE), which was fully characterized using HPLC methods.

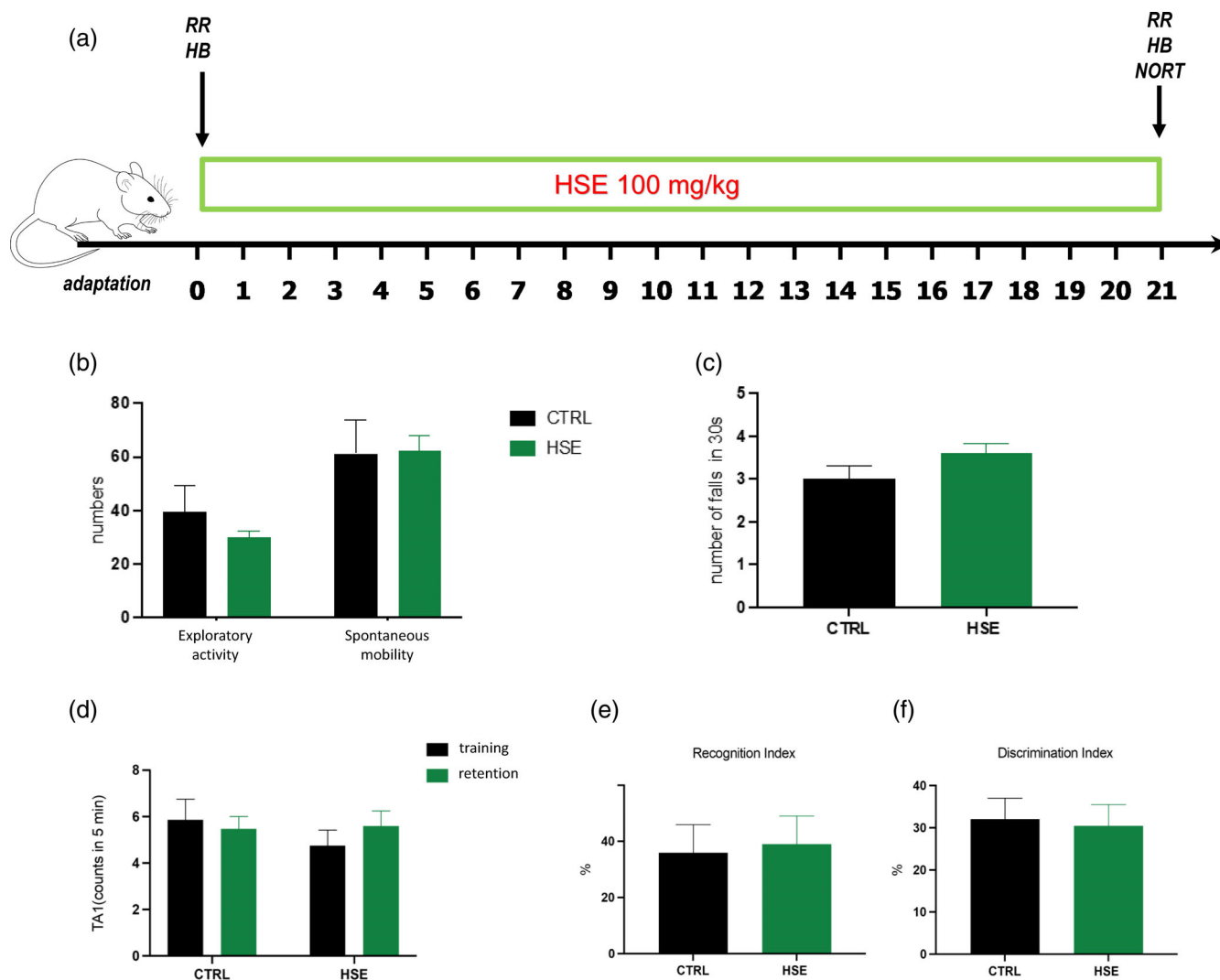


**FIGURE 6** Lack of behavioral side effects by HSE. (a) Schematic representation of the experimental protocol. HB, hole board; NORT, novel object recognition test; RR, rotarod. (b) Lack of alteration of the exploratory activity or spontaneous mobility by HSE repeated treatment. (c) HSE did not induce locomotor impairments in the rotarod test. (d) Lack of effect of HSE on inspection activity in the NORT. (e, f) No effect on the recognition index and discrimination index by HSE. In the NORT, HSE was administered at the dose of 100 mg/kg and experiments were performed on day 21. For all behavioral tests, height mice per group were used.

Only a very limited number of studies on the effect of *Helichrysum* spp. on body weight are available and, to the best of our knowledge, there is still no evidence regarding the activity of *H. stoechas* on feeding behavior. Here, we observed that repeated oral administration of HSE for 3 weeks reduced weight gain in fed mice. Our findings are consistent with previous studies on extracts from *H. italicum*, whose supplementation in overweight insulin-resistant rats can boost the beneficial metabolic effects of caloric restriction, as evidenced by the specific reduction in weight gain (De La Garza et al., 2015). This activity was further confirmed by a very recent clinical study, which has shown that the daily consumption of an infusion of either *H. italicum* or *H. arenarium* in subjects under normal diet with at least two traits of metabolic syndrome produced a reduction in body weight, body mass index, and visceral and total body fat at doses consistent with those used in the present study (Kenig et al., 2022). HSE

did not produce a significant decrease in mouse food intake, but the animal weight gain was less than their pair-fed counterparts suggesting that the decrease in weight gain was not prominently related to the induction of an anorexiatic effect.

In our experiments, we observed that repeated administration of HSE, at the dose effective on modulating feeding behavior, increased the time spent in the center of the arena in the open field (OF) test and prolonged the time spent in the light chamber of the light-dark box (LDB) test compared to the CTRL group, showing an anxiolytic-like activity. Indeed, these behavioral tests are commonly used to assess the animal response toward an anxiety-related environment and allow to identify anxiolytic-like activities of a drug candidate. Of note, the HSE anxiolytic-like effect was obtained after a single administration, in agreement with previous findings (Borgonetti, Les, et al., 2020), and its efficacy progressively increased up to the



completion of the experimentation (3 weeks). These results better defined the anxiolytic-like activity of HSE and they also showed the lack of induction of tolerance to the treatment. Clinically, high comorbidity between anxiety and depression is reported. Thus, we investigated whether HSE could also exert an antidepressant-like effect through the sucrose splash test (SST) and the tail suspension test (TST). HSE was ineffective up to the third week of treatment, when a significant increase in the grooming behavior and a reduction of the immobility time, parameters of an antidepressant-like behavior, were detected. These data indicate that HSE was able to simultaneously control weight gain and emotional behavior, and that an improved efficacy was obtained after repeated administration compared to the acute administration.

Neuroinflammation represents a common etiological mechanism for both obesity and mood disorders (Leng & Edison, 2021). Epigenetic modulation of histone acetylation/deacetylation represents a relevant mechanism to promote and control neuroinflammation (Y. Dai et al., 2021). An emerging role for sirtuins, the class III of histone deacetylases, has been postulated and, among the seven members of the sirtuins family, SIRT1 is the one closely linked with neuroinflammation (Jiao & Gong, 2020). SIRT1 is expressed in both neurons and glial cells (Chen et al., 2005; Hisahara et al., 2008) with a prominent expression in the hippocampus and hypothalamus (Ramadori et al., 2008), brain areas involved in the modulation of mood and body weight, respectively.

In glutamate-exposed SH-SY5Y cells, we observed a significant increase in the SIRT1 protein expression. HSE promoted a neuroprotective effect that was related to a drastic reduction of SIRT1 expression, indicating SIRT1 inhibition as a possible mechanism for HSE. SIRT1 blockade could also be involved in the anxiolytic- and antidepressant-like activity of HSE. Hippocampal samples from mice exposed to an anxiety-related environment showed increased levels of neuronal SIRT1 protein that were drastically reduced by HSE treatment. Accumulating evidence shows that SIRT1 also modulates emotional responses, even if its role is still a matter of controversy. Findings illustrated that SIRT1 in hippocampal neurons mediates anxiety- and depressive-like behaviors in mice (Li et al., 2019). In a mouse model of depression, SIRT1 expression was increased in the nucleus accumbens (NAc) and this overexpression promoted depression- and anxiety-like behaviors. Intra-NAc bilateral infusion of the SIRT1 agonist resveratrol increased anxiety- and depression-like behavior, while SIRT1 knockdown or pharmacological antagonism attenuated those behavioral effects (Kim et al., 2016). Consistently, brain-specific SIRT1-knockout mice have less anxiety-like behaviors than their wild-type littermates, and genetic polymorphisms in *SIRT1* have been found to be associated with anxiety (Libert et al., 2011). Genetic studies (Abe et al., 2011; Kishi et al., 2010) are supported by results from a genome-wide association study (Cai et al., 2015), suggesting that an abnormal level of activity of SIRT1, possibly due to an increase in gene expression, could contribute to depression. SIRT1 polymorphism frequency studies found mutations in depressed subjects that were linked to increased SIRT1 activity (Jansen et al., 2016). Consistent with these

studies, brain-specific *Sirt1*-knockout mice are less susceptible to depression than control mice (Libert et al., 2011).

Concerning the molecular mechanisms, it has been reported that upregulation of SIRT1 leads to anxiety by activating the transcription of monoamine oxidase type A (MAO-A) (Libert et al., 2011), which degrades serotonin and noradrenaline, thus representing an important target in the management of mood disorders. The inhibitory activity of MAO-A enzyme by HSE has been recently described (Les et al., 2017), further supporting the functional correlation between SIRT1 inhibition and anxiolytic behavior. SIRT1 is involved in the control of metabolic processes that regulate body weight. Specifically, the hypothalamic arcuate nucleus (ARC) contains two opposite types of neurons, those that respond to the orexigenic agouty-related peptides (AgRP) promoting food intake, and those that respond to the anorexiogenic proopiomelanocortin (POMC) neuropeptide promoting satiety. On a molecular level, hypothalamic neurons express SIRT1, which is considered an energy sensor (Quiñones et al., 2021). Even though controversy exists on the role of SIRT1 in the regulation of energy metabolism, several studies correlate hypothalamic SIRT1 inhibition to body weight loss in rodents. SIRT-1 blockade by pharmacological inhibitors, including both small interfering RNA-mediated knockdown of SIRT1 in the ARC and specific knockout of SIRT1 in AgRP neurons, decreased feeding behavior (Çakir et al., 2009; Dietrich et al., 2010). In addition, SIRT1 requires the Forkhead Box O1 transcription factor (FoxO1) to control hypothalamic functions. SIRT1, via its deacetylation of FoxO1, positively regulates AgRP transcription increasing food intake, while negatively regulating POMC, inducing satiety (Cyr et al., 2015). Repeated HSE treatment in fed mice reduced FoxO1 expression in the mouse hypothalamus, further supporting the hypothesis of a molecular mechanism involving the inhibition of SIRT1/FoxO1 signaling pathway.

To confirm the SIRT1 inhibitory activity of HSE and to identify the main constituent responsible for this effect, we performed docking simulations and found a possible binding mode for AZL in the inhibitor binding site of SIRT1, which is mediated by the establishment of 4 hydrogen bonds with Arg274, Tyr280, Gln345, and Ile347. Interestingly, the hydrogen bond with the backbone NH of Ile347 is also an important anchor point for the binding of the 4-(4-{2-[(methylsulfonyl)amino]ethyl}piperidin-1-yl) thieno [3,2-d]pyrimidine-6-carboxamide inhibitor (H. Dai et al., 2015), thus suggesting its involvement in the inhibition of SIRT1 and supporting the AZL binding mode hypothesis obtained through docking. Indeed, this interaction was also suggested to be pivotal for the binding of other SIRT1 inhibitors, such as toxoflavin (Choi et al., 2013) and the water-soluble 4-aminomethylated helio-mycin derivative (Lin et al., 2022).

The results from the enzymatic activity assay showed a comparable SIRT1 inhibitory activity for HSE and AZL, and both treatments reduced SIRT1 protein content in *in vitro* studies with comparable efficacy, confirming the SIRT1-mediated molecular mechanism and the prominent role of AZL.

SIRT1 exerts pleiotropic effects at both peripheral and central levels and lacks its function impairs brain activity, such as cognition, learning, and memory formation (Gao et al., 2010). Thus, we

investigated whether HSE produced any behavioral side effects. Repeated administration of the effective dose was devoid of any locomotor alteration or impairment of memory function.

## 5 | CONCLUSIONS

In the present study, we describe for the first time the efficacy of HSE to limit weight gain and to produce anxiolytic-like and antidepressant-like effects. These activities are related to the presence of AZL, which acts as a SIRT1 inhibitor, thus representing a new and promising innovative candidate drug for obesity and associated mood disorders.

## AUTHOR CONTRIBUTIONS

**Vittoria Borgonetti:** Formal analysis; investigation; methodology; writing – original draft. **Clarissa Caroli:** Investigation; methodology; writing – original draft. **Paolo Governa:** Investigation; methodology; writing – original draft. **Brighenti Virginia:** Investigation; methodology. **Federica Pollastro:** Investigation. **Silvia Franchini:** Investigation. **Fabrizio Manetti:** Methodology; writing – original draft. **Francisco Les:** Investigation. **Victor López:** Data curation; investigation. **Federica Pellati:** Conceptualization; data curation; formal analysis; methodology; project administration; resources; supervision; validation; writing – review and editing. **Nicoletta Galeotti:** Conceptualization; data curation; formal analysis; methodology; project administration; resources; supervision; validation; writing – review and editing.

## CONFLICT OF INTEREST STATEMENT

The authors declare no conflict of interest.

## DATA AVAILABILITY STATEMENT

The data presented in this study are available on request from the corresponding author.

## ORCID

Vittoria Borgonetti  <https://orcid.org/0000-0002-2203-5285>

Paolo Governa  <https://orcid.org/0000-0002-5976-780X>

Fabrizio Manetti  <https://orcid.org/0000-0002-9598-2339>

Federica Pellati  <https://orcid.org/0000-0002-9822-6862>

Nicoletta Galeotti  <https://orcid.org/0000-0002-1812-9844>

## REFERENCES

- Abe, N., Uchida, S., Otsuki, K., Hobara, T., Yamagata, H., Higuchi, F., Shibata, T., & Watanabe, Y. (2011). Altered sirtuin deacetylase gene expression in patients with a mood disorder. *Journal of Psychiatric Research*, 45(8), 1106–1112. <https://doi.org/10.1016/j.jpsychires.2011.01.016>
- Amiri, S., & Behnezhad, S. (2019). Obesity and anxiety symptoms: A systematic review and meta-analysis. *Neuropsychiatric*, 33(2), 72–89. <https://doi.org/10.1007/s40211-019-0302-9>
- Blüher, M. (2019). Obesity: Global epidemiology and pathogenesis. *Nature Reviews Endocrinology*, 15(5), 288–298. <https://doi.org/10.1038/s41574-019-0176-8>
- Borgonetti, V., Benatti, C., Governa, P., Isoldi, G., Pellati, F., Alboni, S., Tascadda, F., Montopoli, M., Galeotti, N., Manetti, F., Miraldi, E., Biagi, M., & Rigillo, G. (2022). Non-psychotropic *Cannabis sativa* L. phytocomplex modulates microglial inflammatory response through CB2 receptors-, endocannabinoids-, and NF-κB-mediated signaling. *Phytotherapy Research*, 36(5), 2246–2263. <https://doi.org/10.1002/ptr.7458>
- Borgonetti, V., & Galeotti, N. (2022). Rosmarinic acid reduces microglia senescence: A novel therapeutic approach for the management of neuropathic pain symptoms. *Biomedicine*, 10(7), 1468. <https://doi.org/10.3390/biomedicines10071468>
- Borgonetti, V., Governa, P., Biagi, M., & Galeotti, N. (2020). Novel therapeutic approach for the management of mood disorders: In vivo and in vitro effect of a combination of L-theanine, *Melissa officinalis* L. and *Magnolia officinalis* rehder & E.H. Wilson. *Nutrients*, 12(6), 1803. <https://doi.org/10.3390/nu12061803>
- Borgonetti, V., Les, F., López, V., & Galeotti, N. (2020). Attenuation of anxiety-like behavior by *Helichrysum stoechas* (L.) moench methanolic extract through up-regulation of erk signaling pathways in noradrenergic neurons. *Pharmaceuticals*, 13(12), 1–15. <https://doi.org/10.3390/ph13120472>
- Bruce-Keller, A. J., Keller, J. N., & Morrison, C. D. (2009). Obesity and vulnerability of the CNS. *Biochimica et Biophysica Acta-Molecular Basis of Disease*, 1792(5), 395–400. <https://doi.org/10.1016/j.bbdis.2008.10.004>
- Cai, N., Bigdeli, T. B., Kretschmar, W., Lei, Y., Liang, J., Song, L., Hu, J., Li, Q., Jin, W., Hu, Z., Wang, G., Wang, L., Qian, P., Liu, Y., Jiang, T., Lu, Y., Zhang, X., Yin, Y., Lie, Y., ... Flint, J. (2015). Sparse whole-genome sequencing identifies two loci for major depressive disorder. *Nature*, 523(7562), 588–591. <https://doi.org/10.1038/nature14659>
- Çakir, I., Perello, M., Lansari, O., Messier, N. J., Vaslet, C. A., & Nilni, E. A. (2009). Hypothalamic Sirt 1 regulates food intake in a rodent model system. *PLoS One*, 4(12), e8322. <https://doi.org/10.1371/journal.pone.0008322>
- Cerrato, A., Cannazza, G., Capriotti, A. L., Citti, C., La Barbera, G., Laganà, A., Montone, C. M., Piovesana, S., & Cavaliere, C. (2020). A new software-assisted analytical workflow based on high-resolution mass spectrometry for the systematic study of phenolic compounds in complex matrices. *Talanta*, 209, 120573. <https://doi.org/10.1016/j.talanta.2019.120573>
- Charan, J., & Kantharia, N. (2013). How to calculate sample size in animal studies? *Journal of Pharmacology and Pharmacotherapeutics*, 4(4), 303–306. <https://doi.org/10.4103/0976-500X.119726>
- Chen, J., Zhou, Y., Mueller-Steiner, S., Chen, L. F., Kwon, H., Yi, S., Mucke, L., & Gan, L. (2005). SIRT1 protects against microglia-dependent amyloid-β toxicity through inhibiting NF-κB signaling. *Journal of Biological Chemistry*, 280(48), 40364–40374. <https://doi.org/10.1074/jbc.M509329200>
- Choi, G., Lee, J., Ji, J. Y., Woo, J., Kang, N. S., Cho, S. Y., Kim, H. R., Du Ha, J., & Han, S. Y. (2013). Discovery of a potent small molecule SIRT1/2 inhibitor with anticancer effects. *International Journal of Oncology*, 43(4), 1205–1211. <https://doi.org/10.3892/ijo.2013.2035>
- Cyr, N. E., Steger, J. S., Toorie, A. M., Yang, J. Z., Stuart, R., & Nilni, E. A. (2015). Central sirt 1 regulates body weight and energy expenditure along with the POMC-derived peptide α-MSH and the processing enzyme CPE production in diet-induced obese male rats. *Endocrinology (United States)*, 156(3), 961–974. <https://doi.org/10.1210/en.2014-1970>
- Dai, H., Case, A. W., Riera, T. V., Considine, T., Lee, J. E., Hamuro, Y., Zhao, H., Jiang, Y., Sweitzer, S. M., Pietrak, B., Schwartz, B., Blum, C. A., Disch, J. S., Caldwell, R., Szczepankiewicz, B., Oalman, C., Ng, P. Y., White, B. H., Casaubon, R., ... Ellis, J. L. (2015). Crystallographic structure of a small molecule SIRT1 activator-enzyme complex. *Nature Communications*, 6, 7645. <https://doi.org/10.1038/ncomms8645>
- Dai, Y., Wei, T., Shen, Z., Bei, Y., Lin, H., & Dai, H. (2021). Classical HDACs in the regulation of neuroinflammation. *Neurochemistry International*, 150, 105182. <https://doi.org/10.1016/j.neuint.2021.105182>

- De La Garza, A. L., Etxeberria, U., Haslberger, A., Aumüller, E., Martínez, J. A., & Milagro, F. I. (2015). Helichrysum and grapefruit extracts boost weight loss in overweight rats reducing inflammation. *Journal of Medicinal Food*, 18(8), 890–898. <https://doi.org/10.1089/jmf.2014.0088>
- Dietrich, M. O., Antunes, C., Geliang, G., Liu, Z. W., Borok, E., Nie, Y., Xu, A. W., Souza, D. O., Gao, Q., Diano, S., Gao, X. B., & Horvath, T. L. (2010). AgRP neurons mediate sirt 1's action on the melanocortin system and energy balance: Roles for sirt 1 in neuronal firing and synaptic plasticity. *Journal of Neuroscience*, 30(35), 11815–11825. <https://doi.org/10.1523/JNEUROSCI.2234-10.2010>
- du Sert, N. P., Hurst, V., Ahluwalia, A., Alam, S., Avey, M. T., Baker, M., Browne, W. J., Clark, A., Cuthill, I. C., Dirnagl, U., Emerson, M., Garner, P., Holgate, S. T., Howells, D. W., Karp, N. A., Lazic, S. E., Lidster, K., Mac Callum, C. J., Macleod, M., ... Würbel, H. (2020). The arrive guidelines 2.0: Updated guidelines for reporting animal research. *PLoS Biology*, 18(7), e3000410. <https://doi.org/10.1371/journal.pbio.3000410>
- Erion, J. R., Wosiski-Kuhn, M., Dey, A., Hao, S., Davis, C. L., Pollock, N. K., & Stranahan, A. M. (2014). Obesity elicits interleukin 1-mediated deficits in hippocampal synaptic plasticity. *Journal of Neuroscience*, 34(7), 2618–2631. <https://doi.org/10.1523/JNEUROSCI.4200-13.2014>
- Fagerli, E., Escobar, I., Ferrier, F. J., Jackson, C. W., Perez-Lao, E. J., & Perez-Pinzon, M. A. (2022). Sirtuins and cognition: Implications for learning and memory in neurological disorders. *Frontiers in Physiology*, 13, 908689. <https://doi.org/10.3389/fphys.2022.908689>
- Filaferro, M., Codeluppi, A., Brighenti, V., Cimurri, F., González-Paramás, A. M., Santos-Buelga, C., Bertelli, D., Pellati, F., & Vitale, G. (2022). Disclosing the antioxidant and neuroprotective activity of an anthocyanin-rich extract from sweet cherry (*Prunus avium* L.) using in vitro and in vivo models. *Antioxidants*, 11(2), 211. <https://doi.org/10.3390/antiox11020211>
- Galeotti, N., Sanna, M. D., & Ghelardini, C. (2013). Pleiotropic effect of histamine H4 receptor modulation in the central nervous system. *Neuropharmacology*, 71, 141–147. <https://doi.org/10.1016/j.neuropharm.2013.03.026>
- Galeotti, N., Bartolini, A., & Ghelardini, C. (2006). Blockade of intracellular calcium release induces an antidepressant-like effect in the mouse forced swimming test. *Neuropharmacology*, 50(3), 309–316. <https://doi.org/10.1016/j.neuropharm.2005.09.005>
- Gao, J., Wang, W. Y., Mao, Y. W., Gräff, J., Guan, J. S., Pan, L., Mak, G., Kim, D., Su, S. C., & Tsai, L. H. (2010). A novel pathway regulates memory and plasticity via SIRT1 and mi R-134. *Nature*, 466(7310), 1105–1109. <https://doi.org/10.1038/nature09271>
- Gouveia, S. C., & Castilho, P. C. (2010). Characterization of phenolic compounds in *Helichrysum melaleucum* by high-performance liquid chromatography with on-line ultraviolet and mass spectrometry detection. *Rapid Communications in Mass Spectrometry*, 24(13), 1851–1868. <https://doi.org/10.1002/rcm.4585>
- Heysfield, S. B., & Wadden, T. A. (2017). Mechanisms, pathophysiology, and Management of Obesity. *New England Journal of Medicine*, 376(3), 254–266. <https://doi.org/10.1056/nejmra1514009>
- Hisahara, S., Chiba, S., Matsumoto, H., Tanno, M., Yagi, H., Shimohama, S., Sato, M., & Horio, Y. (2008). Histone deacetylase SIRT1 modulates neuronal differentiation by its nuclear translocation. *Proceedings of the National Academy of Sciences of the United States of America*, 105(40), 15599–15604. <https://doi.org/10.1073/PNAS.0800612105>
- Imai, S. I., Armstrong, C. M., Kaeblerlein, M., & Guarente, L. (2000). Transcriptional silencing and longevity protein Sir 2 is an NAD-dependent histone deacetylase. *Nature*, 403(6771), 795–800. <https://doi.org/10.1038/35001622>
- Jansen, R., Penninx, B. W. J. H., Madar, V., Xia, K., Milaneschi, Y., Hottenga, J. J., Hammerslag, A. R., Beekman, A., Van Der Wee, N., Smit, J. H., Brooks, A. I., Tischfield, J., Posthuma, D., Schoevers, R., Van Grootheest, G., Willemsen, G., De Geus, E. J., Boomsma, D. I., Wright, F. A., ... Sullivan, P. F. (2016). Gene expression in major depressive disorder. *Molecular Psychiatry*, 21(3), 339–347. <https://doi.org/10.1038/mp.2015.57>
- Jiao, F., & Gong, Z. (2020). The beneficial roles of SIRT1 in neuroinflammation-related diseases. *Oxidative Medicine and Cellular Longevity*, 2020, 6782872. <https://doi.org/10.1155/2020/6782872>
- Judzentiene, A., Budiene, J., Nedveckyte, I., & Garjonyte, R. (2022). Antioxidant and toxic activity of *Helichrysum arenarium* (L.) Moench and *Helichrysum italicum* (Roth) G. Don essential oils and extracts. *Molecules*, 27(4), 1311. <https://doi.org/10.3390/molecules27041311>
- Kelly, T., Yang, W., Chen, C. S., Reynolds, K., & He, J. (2008). Global burden of obesity in 2005 and projections to 2030. *International Journal of Obesity*, 32(9), 1431–1437. <https://doi.org/10.1038/ijo.2008.102>
- Kenig, S., Kramberger, K., Šik Novak, K., Karnjuš, I., Bandelj, D., Petelin, A., & Jenko Pražnikar, Z. (2022). *Helichrysum italicum* (Roth) G. Don and *Helichrysum arenarium* (L.) Moench infusions in reversing the traits of metabolic syndrome: A double-blind randomized comparative trial. *Food and Function*, 13(14), 7697–7706. <https://doi.org/10.1039/d2fo00880g>
- Kim, H. D., Hesterman, J., Call, T., Magazu, S., Keeley, E., Armenta, K., Kronman, H., Neve, R. L., Nestler, E. J., & Ferguson, D. (2016). SIRT1 mediates depression-like behaviors in the nucleus accumbens. *Journal of Neuroscience*, 36(32), 8441–8452. <https://doi.org/10.1523/JNEUROSCI.0212-16.2016>
- Kishi, T., Yoshimura, R., Kitajima, T., Okochi, T., Okumura, T., Tsunoka, T., Yamanouchi, Y., Kinoshita, Y., Kawashima, K., Fukuo, Y., Naitoh, H., Umene-Nakano, W., Inada, T., Nakamura, J., Ozaki, N., & Iwata, N. (2010). SIRT1 gene is associated with major depressive disorder in the Japanese population. *Journal of Affective Disorders*, 126(1–2), 167–173. <https://doi.org/10.1016/j.jad.2010.04.003>
- Kramberger, K., Barlič-Maganja, D., Bandelj, D., Baruca Arbeiter, A., Peeters, K., Miklavčič Višnjevec, A., & Pražnikar, Z. J. (2020). HPLC-DAD-ESI-QTOF-MS determination of bioactive compounds and antioxidant activity comparison of the hydroalcoholic and water extracts from two *helichrysum italicum* species. *Metabolites*, 10(10), 403. <https://doi.org/10.3390/metabo10100403>
- Kritis, A. A., Stamoula, E. G., Paniskaki, K. A., & Vavilis, T. D. (2015). Researching glutamate – Induced cytotoxicity in different cell lines: A comparative/collective analysis/study. *Frontiers in Cellular Neuroscience*, 9, 91. <https://doi.org/10.3389/fncel.2015.00091>
- Leng, F., & Edison, P. (2021). Neuroinflammation and microglial activation in Alzheimer disease: Where do we go from here? *Nature Reviews Neurology*, 17(3), 157–172. <https://doi.org/10.1038/s41582-020-00435-y>
- Les, F., Venditti, A., Cásedas, G., Frezza, C., Guiso, M., Sciubba, F., Serafini, M., Bianco, A., Valero, M. S., & López, V. (2017). Everlasting flower (*Helichrysum stoechas* Moench) as a potential source of bioactive molecules with antiproliferative, antioxidant, antidiabetic and neuroprotective properties. *Industrial Crops and Products*, 108, 295–302. <https://doi.org/10.1016/j.indcrop.2017.06.043>
- Li, W., Guo, B., Tao, K., Li, F., Liu, Z., Yao, H., Feng, D., & Liu, X. (2019). Inhibition of SIRT1 in hippocampal CA1 ameliorates PTSD-like behaviors in mice by protections of neuronal plasticity and serotonin homeostasis via NHLH2/MAO-A pathway. *Biochemical and Biophysical Research Communications*, 518(2), 344–350. <https://doi.org/10.1016/j.bbrc.2019.08.060>
- Libert, S., Pointer, K., Bell, E. L., Das, A., Cohen, D. E., Asara, J. M., Kapur, K., Bergmann, S., Preisig, M., Otowa, T., Kendler, K. S., Chen, X., Hetttema, J. M., Van Den Oord, E. J., Rubio, J. P., & Guarente, L. (2011). SIRT1 activates MAO-A in the brain to mediate anxiety and exploratory drive. *Cell*, 147(7), 1459–1472. <https://doi.org/10.1016/j.cell.2011.10.054>
- Lin, M. H., Islam, A., Liu, Y.-H., Weng, C.-W., Zhan, J.-H., Liang, R.-H., Tikhomirov, A. S., Shchekotikhin, A. E., & Chueh, P. J. (2022). Antibiotic

- heliomycin and its water-soluble 4-aminomethylated derivative provoke cell death in T24 bladder cancer cells by targeting sirtuin 1 (SIRT1). *American Journal of Cancer Research*, 12(3), 1042–1055.
- Lumeng, C. N., & Saltiel, A. R. (2011). Inflammatory links between obesity and metabolic disease. *The Journal of Clinical Investigation*, 121(6), 2111–2117. <https://doi.org/10.1172/JCI57132>
- Mao, Z., Gan, C., Zhu, J., Ma, N., Wu, L., Wang, L., & Wang, X. (2017). Anti-atherosclerotic activities of flavonoids from the flowers of *Helichrysum arenarium* L. MOENCH through the pathway of anti-inflammation. *Bioorganic and Medicinal Chemistry Letters*, 27(12), 2812–2817. <https://doi.org/10.1016/j.bmcl.2017.04.076>
- Méndez, D., Escalona-Arranz, J. C., Pérez, E. M., Foubert, K., Matheussen, A., Tuentner, E., Cuyper, A., Cos, P., & Pieters, L. (2021). Antifungal activity of extracts, fractions, and constituents from *Coccoloba cowellii* leaves. *Pharmaceuticals*, 14(9), 917. <https://doi.org/10.3390/ph14090917>
- Michailidou, Z., Gomez-Salazar, M., & Alexaki, V. I. (2022). Innate immune cells in the adipose tissue in health and metabolic disease. *Journal of Innate Immunity*, 14(1), 4–30. <https://doi.org/10.1159/000515117>
- Milaneschi, Y., Simmons, W. K., van Rossum, E. F. C., & Penninx, B. W. (2019). Depression and obesity: Evidence of shared biological mechanisms. *Molecular Psychiatry*, 24(1), 18–33. <https://doi.org/10.1038/s41380-018-0017-5>
- Mopuri, R., & Islam, M. S. (2017). Medicinal plants and phytochemicals with anti-obesogenic potentials: A review. *Biomedicine and Pharmacotherapy*, 89, 1442–1452. <https://doi.org/10.1016/j.biopha.2017.02.108>
- Nogueira Neto, J. D., De Almeida, A. A. C., Da Silva Oliveira, J., Dos Santos, P. S., De Sousa, D. P., & De Freitas, R. M. (2013). Antioxidant effects of nerolidol in mice hippocampus after open field test. *Neurochemical Research*, 38(9), 1861–1870. <https://doi.org/10.1007/s11064-013-1092-2>
- O'Boyle, N. M., Banck, M., James, C. A., Morley, C., Vandermeersch, T., & Hutchison, G. R. (2011). Open Babel: An open chemical toolbox. *Journal of Cheminformatics*, 3(10), 33. <https://doi.org/10.1186/1758-2946-3-33>
- Patel, D. K., & Stanford, F. C. (2018). Safety and tolerability of new-generation anti-obesity medications: A narrative review. *Postgraduate Medicine*, 130(2), 173–182. <https://doi.org/10.1080/00325481.2018.1435129>
- Pugazhenthil, S., Qin, L., & Reddy, P. H. (2017). Common neurodegenerative pathways in obesity, diabetes, and Alzheimer's disease. *Biochimica et Biophysica Acta – Molecular Basis of Disease*, 1863(5), 1037–1045. <https://doi.org/10.1016/j.bbdis.2016.04.017>
- Quiñones, M., Martínez-Grobas, E., Ferno, J., Pérez-Lois, R., Seoane, L. M., & Massadi, O. A. (2021). Hypothalamic actions of SIRT1 and SIRT6 on energy balance. *International Journal of Molecular Sciences*, 22(3), 1–11. <https://doi.org/10.3390/IJMS22031430>
- Ramadori, G., Lee, C. E., Bookout, A. L., Lee, S., Williams, K. W., Anderson, J., Elmquist, J. K., & Coppari, R. (2008). Brain SIRT1: Anatomical distribution and regulation by energy availability. *The Journal of Neuroscience: The Official Journal of the Society for Neuroscience*, 28(40), 9989–9996. <https://doi.org/10.1523/JNEUROSCI.3257-08.2008>
- Sala, A., Recio, M. D. C., Giner, R. M., Máñez, S., Tournier, H., Schinella, G., & Rios, J.-L. (2010). Anti-inflammatory and antioxidant properties of *Helichrysum italicum*. *Journal of Pharmacy and Pharmacology*, 54(3), 365–371. <https://doi.org/10.1211/0022357021778600>
- Sasaki, T., & Kitamura, T. (2010). Roles of fox O1 and Sirt 1 in the central regulation of food intake. *Endocrine Journal*, 57(11), 939–946. <https://doi.org/10.1507/endocrj.K10E-320>
- Tagliatela-Scafati, O., Pollastro, F., Chianese, G., Minassi, A., Gibbons, S., Arunotayanun, W., Mabebie, B., Ballero, M., & Appendino, G. (2013). Antimicrobial phenolics and unusual glycerides from *Helichrysum italicum* subsp. microphyllum. *Journal of Natural Products*, 76(3), 346–353. <https://doi.org/10.1021/np3007149>
- Trott, O., & Olson, A. J. (2009). Auto Dock Vina: Improving the speed and accuracy of docking with a new scoring function, efficient optimization, and multithreading. *Journal of Computational Chemistry*, 31(2), 455–461. <https://doi.org/10.1002/jcc.21334>
- Troubat, R., Barone, P., Leman, S., Desmidt, T., Cressant, A., Atanasova, B., Brizard, B., El Hage, W., Surget, A., Belzung, C., & Camus, V. (2021). Neuroinflammation and depression: A review. *European Journal of Neuroscience*, 53(1), 151–171. <https://doi.org/10.1111/ejn.14720>
- Vujić, B., Vidaković, V., Jadranin, M., Novaković, I., Trifunović, S., Tešević, V., & Mandić, B. (2020). Composition, antioxidant potential, and antimicrobial activity of *helichrysum plicatum* DC. Various extracts. *Plants*, 9(3), 337. <https://doi.org/10.3390/plants9030337>
- Williams, E. P., Mesidor, M., Winters, K., Dubbert, P. M., & Wyatt, S. B. (2015). Overweight and obesity: Prevalence, consequences, and causes of a growing public health problem. *Current Obesity Reports*, 4(3), 363–370. <https://doi.org/10.1007/s13679-015-0169-4>
- Ye, M., Guo, D., Ye, G., & Huang, C. (2005). Analysis of homoisoflavonoids in *Ophiopogon japonicus* by HPLC-DAD-ESI-MSn. *Journal of the American Society for Mass Spectrometry*, 16(2), 234–243. <https://doi.org/10.1016/j.jasms.2004.11.007>

## SUPPORTING INFORMATION

Additional supporting information can be found online in the Supporting Information section at the end of this article.

**How to cite this article:** Borgonetti, V., Caroli, C., Governa, P., Virginia, B., Pollastro, F., Franchini, S., Manetti, F., Les, F., López, V., Pellati, F., & Galeotti, N. (2023). *Helichrysum stoechas* (L.) Moench reduces body weight gain and modulates mood disorders via inhibition of silent information regulator 1 (SIRT1) by arzanol. *Phytotherapy Research*, 37(10), 4304–4320. <https://doi.org/10.1002/ptr.7941>